EFDA–JET–CP(10)08/07

T.C. Hender, G. Arnoux, P. de Vries, S. Gerasimov, A. Huber, M.F. Johnson,
R. Koslowski, M. Lehnen, A. Loarte, J.R. Martín-Solís, V. Riccardo
and JET EFDA contributors

JET Disruption Studies in Support of ITER

JET Disruption Studies in Support of ITER

T.C. Hender[1], G. Arnoux[1], P. de Vries[2], S. Gerasimov[1], A. Huber[3], M.F. Johnson[1], R. Koslowski[3], M. Lehnen[3], A. Loarte[4], J.R. Martín-Solís[5], V. Riccardo[1] and JET EFDA contributors*

JET-EFDA, Culham Science Centre, OX14 3DB, Abingdon, UK

[1]EURATOM-CCFE Fusion Association, Culham Science Centre, OX14 3DB, Abingdon, OXON, UK
[2]FOM Institute for Plasma Physics Rijnhuizen, Association EURATOM-FOM, Nieuwegein, Netherlands
[3]Forschungszentrum Jülich GmbH, Institut für Plasmaphysik, Assoziation-EURATOM, D-52425 Jülich, Germany
[4]ITER Organization, Route de Vinon, CS 90 046, 13067 Saint Paul Lez Durance, France
[5]Laboratorio Nacional de Fusion, Asociación EURATOM-CIEMAT, Madrid, Spain
** See annex of F. Romanelli et al, "Overview of JET Results", (23rd IAEA Fusion Energy Conference, Daejon, Republic of Korea (2010)).*

Preprint of Paper to be submitted for publication in Proceedings of the 23rd IAEA Fusion Energy Conference, Daejon, Republic of Korea (10th October 2010 - 16th October 2010)

ABSTRACT.
Disruptions are a key issue for all future large tokamaks, due to the large mechanical and thermal loads they can place on the vacuum vessel and plasma facing components. This paper summarises recent key advances in understanding on JET, in the disruption area. Results will be presented on halo currents and asymmetric disruptions, where large sideways forces may occur (up to ~4MN in JET) – which are a significant design issue for ITER. Heat loads arising from disruptions are also a concern and JET data on the location, duration and peaking of these heat loads under various classes of disruptions is discussed. Another disruption consequence is Runaway Electrons (REs). IR imaging shows distinct localised impacts on the upper dump plate by the RE beam leading to an increase of the surface temperature of >1000^{o}C; this localization and nature of the runway beam loss is discussed. Intrinsic to mitigation of disruptions is a means to predict that they are going to occur, and results on understanding of the sequence of events that ultimately leads to disruptive termination are outlined. A fast Disruption Mitigation Valve (DMV) has been recently installed on JET to study disruption mitigation by Massive Gas Injection (MGI) and the results are briefly reviewed.

1. INTRODUCTION

Disruptions are a key issue for all future large tokamaks, since the large mechanical and thermal loads they can place on the tokamak structure lead to significant design and operational constraints [1]. It is therefore important to understand their consequences and also the means to avoid or mitigate them. Given that machine size (and field and current) are a key determinant of disruptions loads, JET is well placed to understand ITER disruption issues and this point is further supported by the new disruption mitigation system, improved IR thermal imaging and enhanced magnetic diagnostics (4 octant current moment measurements and halo detectors) on JET.

For ITER key disruption issues are forces on the vessel arising from eddy and halo currents, thermal loads on the first wall and divertor, runaway electron heat loads and disruption mitigation. This paper summarises recent key advances in understanding on JET in these areas.

2. DISRUPTION FORCES

In the vacuum vessel and plasma facing components, disruptions can both induce eddy currents and drive halo currents; the latter flow partly in the plasma completing their circuit through conducting structures surrounding the plasma. Studies for ITER [2] show both sources of wall currents can be significant and that there is limited margin to the resulting Electro-Magnetic (EM) loads. A feature of the halo currents is that they can be non-axisymmetric, resulting in significant non-symmetric forces on the vacuum vessel [3].

Prior to 2005 JET had halo sensors at best at 3 toroidal locations (0^{o}, 90^{o} and 180^{o}) allowing an incomplete determination of the Toroidal Peaking Factor (TPF). Post-2005 with improved poloidal halo diagnostics (at 0^{o}, 90^{o}, 180^{o} and 270^{o}) the analysed JET pulses indicate the previous TPF measurements were on average an underestimate (e.g. by ~0.5 at TPF = 1.7) [4], but the product,

I_{halo}/I_p * TPF remains well within the ITER design guideline of 0.75.

In addition to poloidal halo current asymmetries, also observed are toroidal variations in the toroidal plasma current (I_p) [5]. The JET data show a clear relationship between the poloidal halo currents and I_p asymmetries [4], but a full understanding remains to be developed. The I_p asymmetries are known to be associated with sideways forces on the vessel [6], which can be very significant in JET (up to ~4MN). An empirical model (the sink and source model [6]) has been developed to explain these sideways forces and is employed for force calculations in ITER [3]. Therefore significant effort is being devoted to understanding and quantifying this I_p asymmetry, which is observed as an n~1 variation of plasma current and first plasma current vertical moment [7].

A proposed theoretical explanation of the I_p asymmetries is that an $m = n = 1$ kink mode causes helical surface currents [8], and these currents have part of their path in the wall as the kink mode intercepts the wall, but a full quantitative description remains to be developed - an accurate calculation of the sideways forces requires an appropriate wall model linked to a kink mode evolution model, which would determine the evolution of mode amplitude as well as the forces.

On JET the toroidal asymmetries of the plasma current, and its moments, are measured using arrays of in-vessel poloidal field pick-up coils and ex-vessel saddles at 4 toroidal locations (termed octants 1, 3, 5 and 7) each separated by 90°. In the present JET disruption database there are 954 pulses with reliable data at the 4 toroidal locations and 4457 pulses with reliable data from 2 opposite toroidal locations (octants 3 and 7) – it should be noted this database [7] includes disruptions, with $I_p^{dis} \geq 1$MA, from all causes, not just Vertical Displacement Events, VDEs (where I_p^{dis} is the pre-disruptive plasma current). To systematically quantify the plasma current asymmetries the following quantity is used:-

$$A_{4Oct} = \frac{1}{I_p^{dis}} \int I_p^{asym}\, dt$$

where I_p^{dis} = pre-disruptive plasma current and $I_p^{asym} = \sqrt{(I_7 - I_3)^2 + (I_1 - I_5)^2}$ with I_1= octant 1 plasma current etc. To avoid noise contributing to the results, the $A_{4\,oct}$ integral is only evaluated for times when $|I_p^{asym}|$>10kA and $|_p^{asym}|$>0.5% $|I_p^{dis}|$ and $|I_p|$>10% $|I_p^{dis}|$. In the results presented the time of disruption is defined as the point when $|dI_p/dt|$>25MA/s for at least 2ms for VDEs, or the peak of the negative loop voltage spike for disruptions that occur before vertical instability onset. I_p^{dis} is then defined as the average I_p over 20-50ms before the disruption time.

It is important to note that $A_{4\,oct}$ is a measure of the peak-to-peak variation, and not the amplitude of plasma current asymmetry. Ignoring transients then $A_{4oct} \sim \int F_{asym} dl$ (dl $_p B_t$) where F_{asym} is the asymmetric force and a the minor radius. So $A_{4\,oct}$ is related to the magnitude of the asymmetric impulse force.

In cases where just octant 3 and 7 data are available then a 2 octant asymmetry $A_{2\,oct}$ can be defined. If the asymmetric currents (I_7-I_3 and I_5-I_1) are assumed as a pure sine waves in time then

$$A_{4Oct} = \pi/2\, A_{2Oct}$$

Figure 1 shows the variation of $A_{4\ oct}$ for the whole 954 shot 4 octant database and the variation of $A_{2\ oct}$ for the whole 2 octant database. Also shown is the $\pi/2\ A_{2\ oct}$ together with $A_{4\ oct}$ for shots where 4 octant data are available – it can be seen on average that $\pi/2\ A_{2\ oct}$ gives a good description of the 4 octant data.

There is a significant difference in the asymmetry between upward and downward going VDEs in JET. The upward going VDEs have a peak $\pi/2*A_{2oct}$= 3.67ms whereas the downward going VDEs have a peak of 1.34ms; the reason for this difference is not clear but presumably depends on the machine magnetic and physical geometry.

The traces of I_p^{asym} / I_p^{dis} for the cases with largest values of $A_{4\ oct}$ and $A_{2\ oct}$ are shown in Fig 2. In these plots $t = 0$ is defined such that $\int_{t<0} I_p^{asym} dt = \int_{t>0} I_p^{asym} dt$. Under the previously developed ITER specification for the I_p asymmetry [9] a +/-2ms rectangular smoothing of the JET data was applied, on the basis that such short timescale behaviour (when extrapolated to ITER) will have no mechanical effects. Given the ~8Hz ITER vessel frequency the choice of +/-2ms smoothing time (though somewhat arbitrary) is conservative (how to extrapolate timescales to ITER is discussed below). It can be seen from Fig 2 (left) that with the 2ms smoothing the previously developed envelope [9] (I_p^{asym} / I_p^{dis}=10% for 37.5ms) is reasonable for the 4 octant data. For the 2 octant data, in terms of impulse, $(\pi/2)A_{2\ oct}$ is closely bounded by 3.75ms. However the 2 octant data in Fig.2 show the 37.5ms window does not fully envelope the data; though it does cover the central peaks as shown in Ref [9]. A very conservative choice would be a 10% envelope for 55ms (though in terms of impulse a 37.5ms envelope of I_p^{asym} / I_p^{dis}=10% is adequate)

This lengthening of envelope between the 4 and 2 octant data, corresponds to some pulses with longer current quenches at high values of $A_{2\ oct}$, which are not in the 4 octant database (Fig 3). Since the duration of the I_p asymmetry is always within the current quench duration, the quench data is consistent with the lengthening of the I_p asymmetry between the 4 and 2 octant data. The line in Fig.3, which provides a good bound on the data, corresponds to $I_p^{asym} / I_p^{dis} = 10\%$ for the whole current quench duration. Also since the I_p quench duration is known to scale linearly with plasma area [1], this possibly justifies scaling the asymmetry duration with plasma area – implying the asymmetries will persist a factor of ~5 times longer in ITER than JET.

The ITER IO use a specification of disruptions that are divided into the worst 6% of asymmetric VDEs (termed Cat III/IV) and the least bad 94% (termed Cat II). For the 4 octant data using $A_{4\ oct}$ as the asymmetry measure to define the CAT III to CAT II boundary, this occurs at 1.18ms; giving a ratio of the peak CAT III/IV to CAT II I_p asymmetries of 2.15/1.18 = 1.82. The equivalent ratio for the 2 octant dataset is rather bigger at 3.67/1.44 = 2.55; giving a measure of uncertainty in the result.

In the majority of pulses the halo and I_p asymmetry rotates counter to I_p, at ~100Hz, though there is significant scatter and a few pulses even rotate in the I_p-direction [7]. For the ITER vessel the most problematic rotation frequency is ~8Hz, the fundamental mechanical vessel frequency. Rotating modes resonating with the vessel frequency will lead to dynamic amplification of the structural forces Figure 4 shows the number of revolutions calculated for four different time

windows specified by condition I_p^{asym} / I_p^{dis} ($\equiv A_p^{asym}$)>0.5%, 1%, 2% and 5% for first and last window time points. The degree of rotation is in the range from -2 turns to +8 turns for the entire 4 octant database, where plasma current and the toroidal field are in the anticlockwise (negative) direction. The physical processes leading to these rotation variations are not presently understood, however at the ITER vessel frequency (~8Hz) around 2 turns are expected through the duration of the peak CAT III/IV events, limiting dynamic amplification.

3. HEAT LOADS

A second significant consequence of disruptions is the resulting thermal loads. InfraRed (IR) data have been collected with a wide angle fast camera (1ms) on the upper dump plate, inner and outer wall, and a new ultra fast (86μs) camera on the divertor during discharges ending in 4 types of disruptions: density limit, radiative collapse, low-q static X-point and upward vertical displacement. In order to meet the 1ms timescale needed to resolve the disruption heat loads the region of interest viewed (inner wall, outer wall etc) must be shifted on a shot by shot basis. Figure 5 shows an example of a set of low-q disruptions ($q_{95}\approx 2$); it can be seen that the timescales of the heat loads to the divertor and outer limiter are comparable and within the thermal quench phase. Given the plasma moves inwards during the disruption this is evidence of a broadened scrape-off layer, causing thermal loads on the outer limiter. Also it can be seen in Fig 5 that a substantial heat load (>5MW/m^2) is deposited on the inner and outer limiters during the current quench phase.

For ITER a key issue is any localisation of the heat loads. In JET the improved bolometer camera system allows a good diagnosis of the poloidal peaking [10]. The strongest localisation of the radiation heat load occurs during VDEs on the upper dump plate (Fig.6). This localisation during VDEs can be reduced using Massive Gas Injection (MGI). In this case it is found that the peak heat load on the dump plate reduces from 3.3MW/m^2 to 1.8MW/m^2, when MGI is employed [10,11].

4. RUNAWAY ELECTRONS

A third disruption consequence is Runaway Electrons (RE). In ITER RE currents of up to ~10MA, (i.e. 70% of the pre-disruption current) are predicted with an average energy of ~10MeV [1]. These RE currents are far larger than in JET, where typically ~1MA is observed (though historically up to 2.5 MA of RE current has been observed). Nevertheless the effects of RE loss in JET are significant enough to be observable allowing our physics understanding to be advanced.

The low assimilation and fast I_p decay associated with pure Ar or pure Ne, Massive Gas Injection (MGI) triggered disruptions of ohmic X-point plasmas leading to distinct runaway plateaus in I_p. In 17 such disruptions distinctive localised heating of the upper dump plate in 5 spots is observed by the IR camera (Fig.7).

The location of the 5 hot spots is due to small inaccuracies in the tile positioning as opposed to plasma asymmetries. Four of the hot spots appear on the same row of dump plate tiles, the fifth on the next row. Due to the unevenness of the dump plate tiles the wetted area is 0.3-0.5m^2

(assuming the pattern observed in the viewed octant is repeated). Typically in these disruptions the initial heat rise on the 5 tiles at the thermal quench is much smaller than that following the RE loss (a factor of ~5). A correlation of average tile temperature rise as $I_{RE}^{2\pm0.6}$ has been found [12] and this is consistent with Ohmic heating of the tile surface to the depth of RE penetration [13] or with significant conversion of the beam magnetic energy to kinetic energy at the beam termination (see below).

The effects of applied non-axisymmetric n = 1 or n = 2 fields on the runaway beam have been studied in JET [11] (up to $\delta B_r/B_T \approx 10^{-3}$ for n = 1 and 2×10^{-3} n = 2, though the values are lower at resonant surfaces [11]); at these values no appreciable effect on the runaway confinement is observed, consistent with modelling due to the supra-thermal orbit widths. Also TF ripple to the level of $\delta b_T/B_T = 1.2\%$ at the outer mid-plane does not affect RE confinement [11]. The routes by which the runaway beam's magnetic energy is ultimately lost are being studied [14]; the magnetic energy of the runaway beam is typically 3-10× larger than its kinetic energy. It is found that a negligible amount (<10%) is lost as radiation as the RE beam quenches, with the other main possible loss routes being conversion to kinetic energy of the REs or conversion to current/magnetic energy in the background plasma. Direct analysis of the data shows that ~20-100% of the RE current is converted to thermal plasma current. Modelling of 2 extreme cases corresponding to observed behaviour is consistent with the observed range of post-runaway thermal current: (a) single main RE loss event with a thermal plasma background at 9eV, (b) a repeated burst-like loss of the REs whose characteristics are taken from Pulse No: 63117. The modelling shows in case (a) 18% of the magnetic energy is converted RE kinetic energy while in case (b) 81% is converted. Since the runaway energy is deposited in local hotspots (Fig.7) and because of their high energy they deposit deeper into components, even a few tenths of the magnetic energy being converted to RE kinetic energy is a significant effect.

5. DISRUPTION MITIGATION, CAUSES AND DETECTION

In order to devise proper strategies to prevent disruptions, knowledge of the root-causes that set in motion the events that lead to disruption, is important. At JET 2309 disruptions over the last decade of operations have been analysed in detail [15]. The largest fraction had an NTM as root-cause, closely followed by disruptions caused by operator error. More than half of them were caused by a technical problems such as density control errors or failure of heating systems. Hence, in order to prevent disruptions, one has to focus attention on eliminating or reducing these specific causes.

A fast valve (Disruption Mitigation Valve- DMV) has been recently installed on JET to study disruption mitigation by MGI and latest results are presented in [16]. A significant reduction of VDE forces (halo current fraction reduced by up to ~4) has been achieved with MGI [16,17], along with reduced poloidal localisation of heat loads (as discussed in Section 3). However, as noted above the gas mixture needs to be chosen to avoid inducing runaways. As yet the MGI densities achieved are a small fraction (~2%) of values needed to avoid secondary runaways [1].

SUMMARY

JET data concerning the magnitude and rotation of I_p asymmetries during disruptions, providing a basis for detailed modelling of asymmetric vacuum vessel forces in ITER [3], has been presented. The amplitude of the I_p asymmetry in JET is <~10% of the pre-disruptive I_p and has a maximum duration at peak of ~40-60ms in JET (which would extrapolate to ~200-300ms in ITER). The heat loads during disruptions have been measured using IR imaging, and it is found that there is significant broadening of the outboard scrape-off layer, allowing comparable heat loads to the outboard wall and divertor. It is found that the most poloidally peaked heat loads occur on the upper dump plate during upward moving VDEs, though this is mitigated by MGI. Runaway electrons are found to be lost to small wetted areas determined by small tile misalignments/irregularities and it is found that a significant fraction of the runaway beam magnetic energy (typically several 10's of percent) can be converted to kinetic energy of the runaway beam during its quench. Promising results on means to detect impending disruptions and mitigate them using massive gas injection have been briefly discussed. Overall there has been significant progress in the understanding of disruptive behaviour likely in ITER.

ACKNOWLEDGEMENTS

This work, part-funded by the European Communities under the contract of Association between EURATOM and CCFE, was carried out within the framework of the European Fusion Development Agreement. The views and opinions expressed herein do not necessarily reflect those of the European Commission. This work was also part-funded by the RCUK Energy Programme under grant EP/G003955.

REFERENCES

[1]. T.C. Hender et al, 'Chapter 3: MHD stability, operational limits and disruptions', Nuclear Fusion **47** (2007) S128

[2]. M. Sugihara et al, 'Disruption scenarios, their mitigation and operation window in ITER', Nucl. Fusion **47** (2007) 337

[3]. C. Bachmann, 'Specification of asymmetric VDE loads of the ITER tokamak', SOFT conference 2010 (to be published Fus Eng and Design)

[4]. V. Riccardo et al, 'Progress in understanding halo current at JET' Nuclear Fusion **49** (2009) 055012

[5]. P Noll et al, in Proceedings of the 19th Symposium on Fusion Technology, Lisbon, 1996 , Vol. 1, p. 751

[6]. V. Riccardo et al, 'Forces between plasma, vessel and TF coils during AVDEs at JET' Nuclear Fusion **40** (2000) 180

[7]. S.N. Gerasimov et al, 'Scaling JET disruption sideways forces to ITER' EPS 2010 Dublin, P4.121

[8]. L. Zakharov, 'The theory of the kink mode during the vertical plasma disruption events in tokamaks' Physics of Plasma **15** (2008) 062507

[9]. C. Bachmann, ITER Report ITER_D_2DJ5AA V2.7 (2009)

[10]. A. Huber et al, 'Radiation loads onto plasma-facing components of JET during transient events – experimental results and implications for ITER', submitted Journal of Nuclear Materials (2010)

[11]. V. Riccardo et al, 'JET disruption studies in support of ITER', submitted to Plasma Physics and Controlled Fusion 2010.

[12]. G. Arnoux, 'Heat load measurements on the JET first wall during disruptions', PSI conference paper O-31, 2010 (to be published Jnrl Nucl Materials)

[13]. B. Bazylev et al, 'Modeling of runaway electron beams for JET and ITER' PSI conference paper P1-98, 2010 (to be published Journal of Nuclear Materials)

[14]. A. Loarte et al, 'Magnetic energy flows during the current quench and termination of disruptions with runaway current plateau formation in JET and implications for ITER' submitted to Nuclear Fusion

[15]. P de Vries et al, 'Survey into the occurrence of disruptions and their root causes at JET', this conf EXS/P2-04

[16]. M Lehnen et al, 'Disruption Mitigation by Massive Gas Injection in JET' this conference EXS/P2-13

[17]. S.A. Bozhenkov et al, 'JET Experiments on Massive Gas Injection', 51st APS Meeting Atlanta, 2009

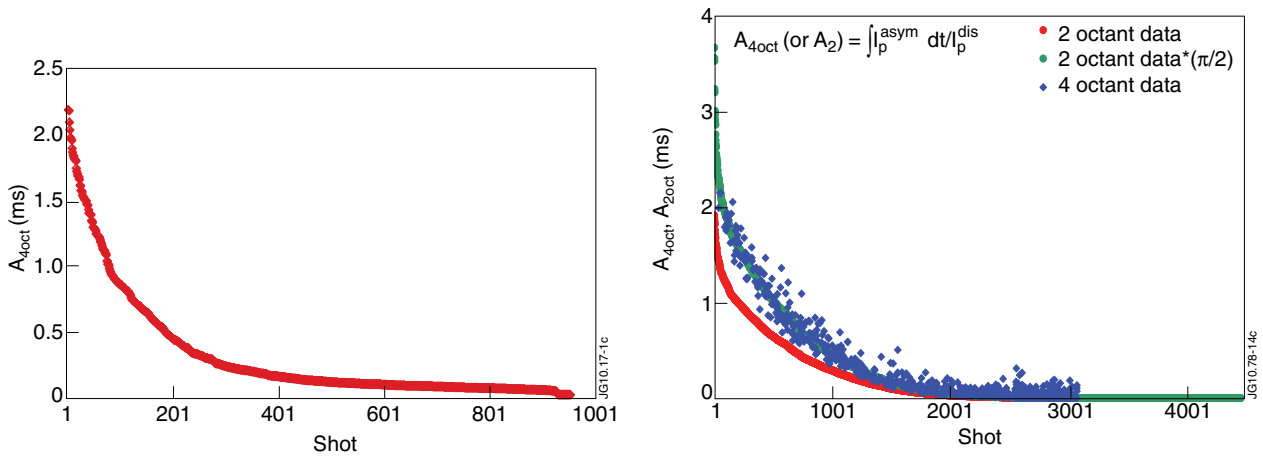

Figure 1: Left-hand plot shows A_{4oct} for the whole 4 octant database (with data sorted into descending order). The right-hand plot shows the entire 2 octant database (red), data for 4 octant shots (blue) where it exists, and π/2 $A_{2\ oct}$ (green). In the right-hand plot the data are sorted by descending size of $A_{2\ oct.}$

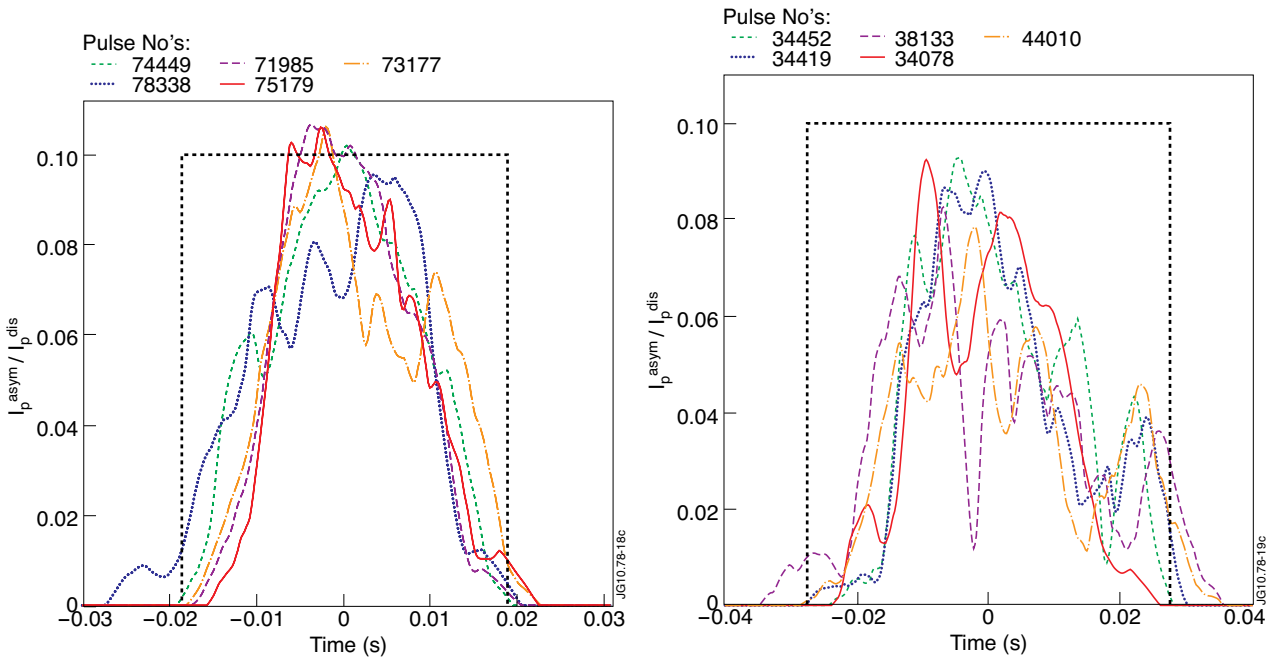

Figure 2: I_p^{asym}/I_p^{dis} for pulses with the maximum $A_{4\,oct}$ values (left hand figure) and maximum A_{2oct} values (right hand figure). The data are smoothed with a +/-2ms rectangular window.

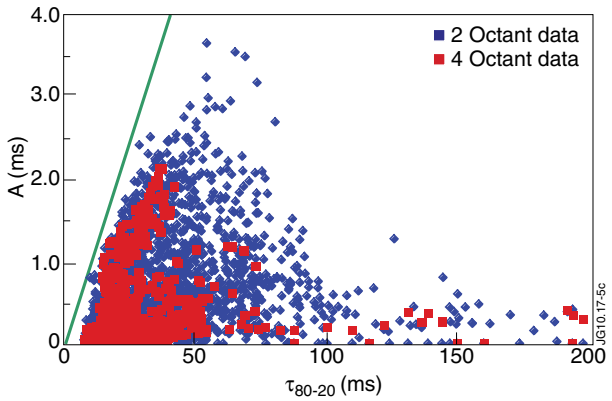

Figure 3: A_{4oct} (red) and $\pi/2$ $A_{2\,oct}$ (blue) vs the current quench time extrapolated from time to quench from 80 to 20% of I_p^{dis} (ie. the time from 80 to 20% multiplied by 5/3). The green line is the integral asymmetry if the I_p asymmetry is 10% of I_p for the whole $\tau_{80\text{-}20}$ time.

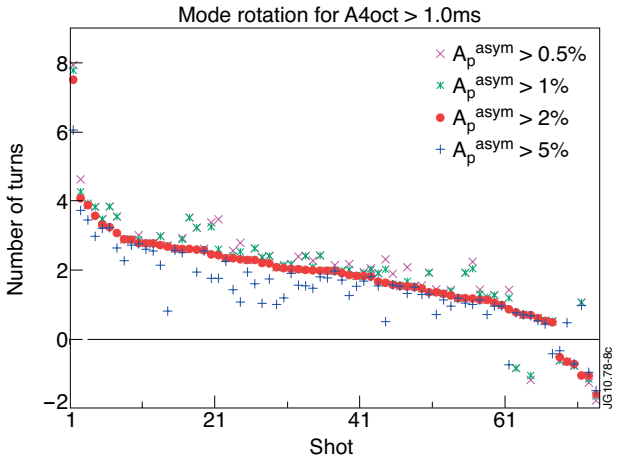

Figure 4: The number of turns calculated for 4 octant databases.

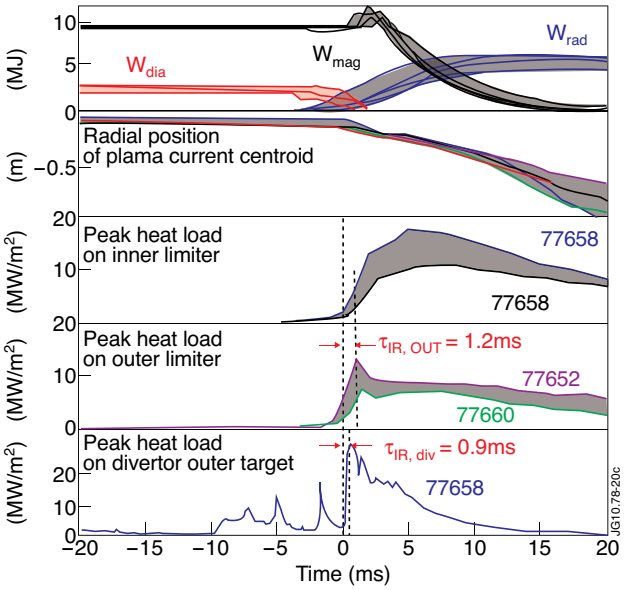

Figure 5: (a) the thermal, W_{th}, magnetic, W_{mag} and radiated, W_{rad} energies during the 40ms around the thermal quench (t=0). (b) the radial position of the current centroid with respect to the major radius, R_0. (c) to (e) the peak heat load measured on the inner limiter, outer limiter and outer target of the divertor respectively.

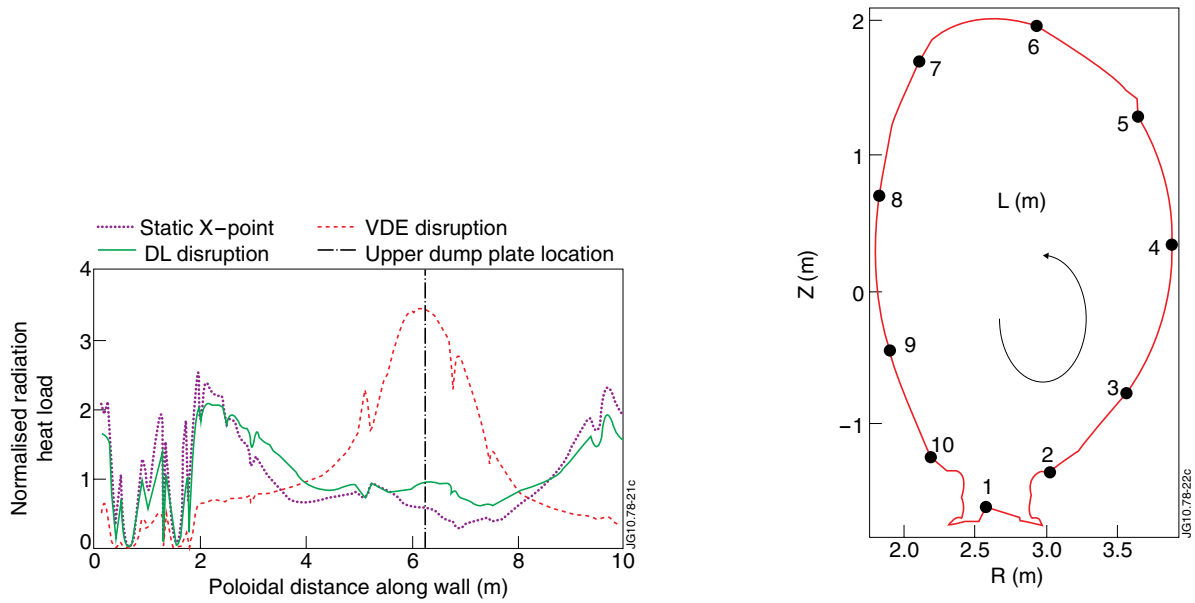

Figure 6: Normalised Radiation Heat load during thermal quench as function of poloidal distance around the wall (as defined in the right figure) for disruptions caused by a density limit, Neo-classical Tearing Mode (NTM) and a VDE. The heat loads are normalised by their average values [10].

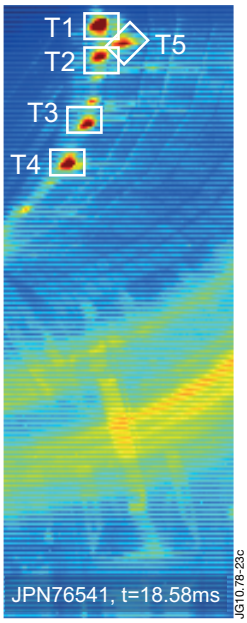

Figure 7: IR view showing 5 tiles being heating strongly during the phase in which the RE current is lost.